# Ternary Semiconductors and Ordered Pseudobinary Alloys: Electronic Structure and Predictions of New Materials

ALEX ZUNGER

*Solar Energy Research Institute, Golden, Colorado 80401, USA*

## Abstract

Using the tools of self-consistent band theory and *ab-initio* total energy calculations for solids we analyze the band gap anomalies in ternary chalcopyrites (e.g., $CuGaS_2$) and pseudobinary alloys (e.g., $In_xGa_{1-x}P$) and predict hitherto unknown new ternary crystals (e.g., $MgGeAs_2$) as well as the existence of *ordered* stable crystals of binary alloys (e.g., $GaAlS_2$, $InGaP_2$).

## I. Introduction

For a large number of applications in electro-optical semiconductor devices, a particular value for the semiconductor energy band gap $E_g$ is often required. While this value depends on one particular application at hand (e.g., Infrared detectors, solid state lasers, or photovoltaic solar cells), existing binary semiconductors, of the IV–IV variety (e.g., Si, Ge), the III–V class (e.g., GaAs, InP) or the II–VI class (e.g., CdTe, HgTe, ZnSe) offer but a limited series of discrete values of $E_g$. The principal method for obtaining a desired value of $E_g$ has traditionally been the use of *ternary*, rather than *binary* semiconductor; the added chemical degree of freedom is then used to obtain a tailor-made band gap. There are two broad classes of ternary semiconductors used to achieve a desired value of $E_g$. The first [1] is the group commonly referred to as ''pseudobinaries'', i.e., a *mixture* of two binary materials with a common element. For example, an alloy of GaAs and InAs produces the pseudobinary $Ga_xIn_{1-x}As$ system where $0 \leqslant x \leqslant 1$ is the mole fraction of GaAs. As grown, these structures are random, in that the alloyed elements are not ordered crystallographically. The second group is the true ternary crystals. For example, much like AlP can be thought of as being related to Si by transfer of a nucleon from one silicon atom to the other (i.e., $^{14}Si + {}^{14}Si \rightarrow {}^{13}Al + {}^{15}P$), so can the ternary system $CuGaS_2$ be thought of as evolving from the binary system ZnS by a transfer of a nucleon from one Zn to the other (i.e., $^{30}ZnS + {}^{30}ZnS \rightarrow {}^{29}Cu\,{}^{31}GaS_2$). In this way we can create two groups of true ternary systems [2], evolving generically from the II–VI and III–V binary groups, respectively. The first is the ternary chalcopyrites $A^IB^{III}C_2^{VI}$, with $A^I = Cu,Ag$, $B^{III} = Al,Ga,In$, and

International Journal of Quantum Chemistry: Quantum Chemistry Symposium 19, 629–653 (1986)

CCC 0360-8832/86/010629-25$04.00

$C^{VI}$ = S,Se, and Te. The second is the ternary pnictides $A^{II}B^{IV}C_2^V$ with $A^{II}$ = Zn,Cd,Hg, $B^{IV}$ = Si,Ge,Sn and $C^V$ = P,As and Sb. Other, more complex systems are possible (c.f. Sec. II), but we will concentrate here mostly on these simpler groups. Both the pseudobinaries and the ternary chalcopyrite and pnictide groups have a zincblende-like fourfold tetrahedral coordination, like their parent materials. They also share in common the fact that their band gaps are not related linearly to those of their parent binary materials. Denoting by $\bar{E}_g(x) \equiv xE_g(AC) + (1-x)E_g(BC)$ the linearly weighted-average of the band gaps of two binary ($AC$ and $BC$) systems, the actual observed band gap $E_g(x)$ of the $A_xB_{1-x}C$ random alloy can usually be fitted [1] to the form

$$E_g(x) \equiv \bar{E}_g(x) - b\,x(1-x)\ ,$$

where $b$ is termed the "optical bowing parameter." Its value is usually positive for the lowest-lying band gaps, and ranges for III–V materials around $0 \leq b \leq 0.9$ eV and in the range of $0 \leq b \leq 1.4$ eV for II–VI systems. Figure 1 shows the observed [3] $E_g(x)$ curves for pseudobinary zinc chalcogenides, exhibiting both the smallest ($ZnS_xSe_{1-x}$) and the largest ($ZnSe_xTe_{1-x}$) bowing ever observed in isovalent semiconductor alloys. An analogous phenomenon occurs in ternary crystals: Table I shows that ternary systems have band gaps that fall considerably below the values of their binary analogs i.e., the ternaries too have positive bowing parameters.

Traditionally, the two phenomena—anomalously small band gaps in $A_xB_{1-x}C$

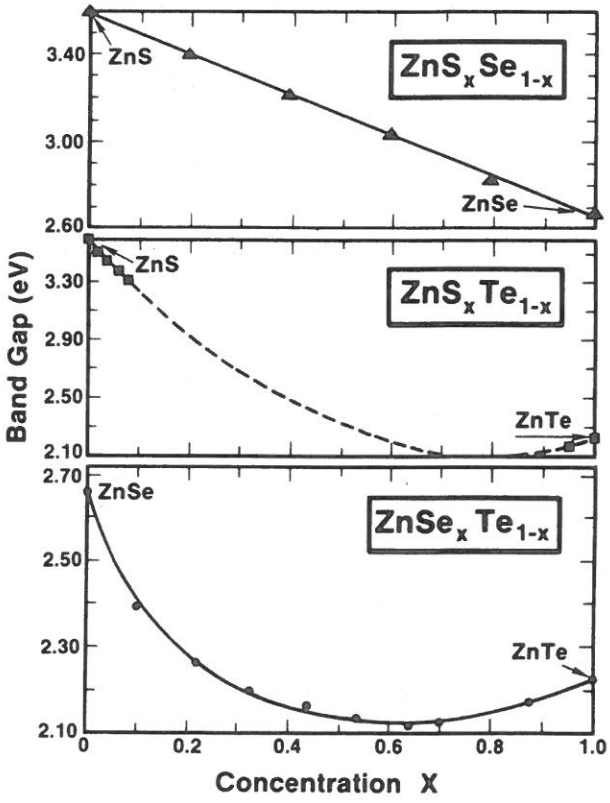


Figure 1. Observed [3] composition-variation of the optical gaps in pseudobinary zinc chalcogenides.

TABLE I. The observed band gaps of ternary semiconductors $E_g^{(3)}$ and the difference $\Delta E_g \equiv E_g^{(2)} - E_g^{(3)}$ (band gap anomaly) with respect to the binary analogs. Uncertain values are denoted by an asterisk. Data are from Reference 2 and references therein.

| Ternary | Ternary Band Gap $E_g^{(3)}$ (eV) | Binary Analog | Band Gap Anomaly $\Delta E_g$ (eV) |
|---|---|---|---|
| $CuAlS_2$ | 3.49 | $Mg_{.5}Zn_{.5}S$ | 2.41 |
| $CuGaS_2$ | 2.43 | ZnS | 1.37 |
| $CuInS_2$ | 1.53 | $Zn_{.5}Cd_{.5}S$ | 1.64 |
| $CuAlSe_2$ | 2.67 | $Mg_{.5}Zn_{.5}Se$ | 1.47 |
| $CuGaSe_2$ | 1.68 | ZnSe | 1.00 |
| $CuInSe_2$ | 1.04 | $Zn_{.5}Cd_{.5}Se$ | 1.29 |
| $CuAlTe_2$ | 2.06 | $Mg_{.5}Zn_{.5}Te$ | 1.44 |
| $CuGaTe_2$ | 1.23 | ZnTe | 1.06 |
| $CuInTe_2$ | 0.96-1.06 | $Zn_{.5}Cd_{.5}Te$ | 0.98-0.88 |
| $AgAlS_2$ | 3.13 | -- | -- |
| $AgGaS_2$ | 2.51-2.73 | $Zn_{.5}Cd_{.5}S$ | 0.62-0.44 |
| $AgInS_2$ | 1.87 | CdS | 0.66 |
| $AgAlSe_2$ | 2.55 | -- | -- |
| $AgGaSe_2$ | 1.83 | $Zn_{.5}Cd_{.5}Se$ | 0.50 |
| $AgInSe_2$ | 1.24 | CdSe | 0.61 |
| $AgAlTe_2$ | 2.27(*) | -- | -- |
| $AgGaTe_2$ | 1.1-1.326(*) | $Zn_{.5}Cd_{.5}Te$ | 0.84-0.62 |
| AgInTe2 | 0.96-1.04(*) | CdTe | 0.62-0.54 |

random alloys and in ternary $ABC_2$ crystals—have not been recognized as being related. The physics of pseudobinary alloys has been discussed in terms of randomness and disorder phenomena [1], and that of ternary semiconductors has been dealt with within the language of band theory of ordered crystals. In this paper I point to the fact that the two phenomena share in common the same physical origin, and that analysis of this mechanism allows us to predict new, hitherto unrecognized ternary systems, of potential technological interest.

## II. Structural Models

Assume that we combine two fourfold coordinated binary systems $AC$ and $BC$ that have a common element to create a new, fourfold coordinated lattice. Which ordered spatial arrangements are possible for integer mixing ratios? If we use Landau's theory [4], of order-disorder phase transitions, we can identify a few structures which can

disorder into the zincblend structure. Four of these structures are shown in Figure 2, along with the zincblend structure. The general empirical formula for such compounds is $A_{4-n}B_nC_4$ where $n=0,1,2,3$ and 4 is the number of $B$ atoms. For $n=0$ and 4 we have the regular zincblend structures $A_4C_4 \equiv 4AC$ and $B_4C_4 = 4BC$. For $n=2$ we have two $ABC_2$-like structures: the chalcopyrite and the simple tetragonal structure. For $n$ either 1 or 3 we again have two $A_3BC_4$ (or $AB_3C_4$) structures: the Luzonite and the Famatinite. Figure 2 shows their Bravais lattices, space groups, atomic positions and allowed diffraction patterns. We hence see that in addition to the known chalcopyrites and pnictides, other structural forms are possible. Three of the most likely forms are shown in Figure 2. Two of them (Luzonite and Famatinite) are naturally occuring minerals. Each structure is characterized by two types of anion-cation bond lengths, $R_{AC}^{(n)}$ and $R_{BC}^{(n)}$. In general, those bond lengths (and the corresponding bond angles) could be deformed relative to the ideal bond lengths $d_{AC}^0 = \frac{\sqrt{3}}{4} a_{AC}^0$ and $d_{BC}^0 = \frac{\sqrt{3}}{4} a_{BC}^0$ of the constituent binary crystals $AC$ and $BC$ at their equilibrium lattice constant $a_{AC}^0$ and $a_{BC}^0$, respectively. Call these deviations $\Delta_{AC}^{(n)} = R_{AC}^{(n)} - d_{AC}^0$ and $\Delta_{BC}^{(n)} = R_{BC}^{(n)} - d_{BC}^0$. Clearly, in comparing an alloy to its end-point materials we have to consider the fact that not only could the two have different atomic volumes, but that even for a fixed volume, alloys, in contrast to their parent materials, may have $\Delta_{AC} \neq 0$, $\Delta_{BC} \neq 0$. Note that if the cations $A$ and $B$ were on a fixed fcc lattice, like in their parent binary materials, then the various $\Delta^{(n)}$ parameters would have been related, e.g., $\Delta_{AC}^{(2)} = \Delta_{BC}^{(2)}$, etc. This appears to be so, to within a good approximation, as indicated by recent EXAFS (extended x-ray absorption fine structure) experiments [5].

## III. Band Structure of Ternary Chalcopyrites

The self-consistent band structure of a typical chalcopyrite—$CuInSe_2$—is given in Figure 3. This band structure has been calculated [2] by the Mixed-Basis Potential Variation (MBPV) method [6], in which no shape approximation is applied to the potential, all core and valence electrons are treated dynamically (i.e., no pseudopotentials), a mixed basis set consisting of about 400 symmetrized plane waves plus 126 compressed-atom radial orbitals are used, and self-consistency is achieved to within 1 mRy, using the Jacobian Update method [6]. Since we use the local density form of the Hamiltonian, not surprisingly, the band gap comes out to be too small (Fig. 3a). Using Slater's exchange (Fig. 3b) results in a larger band gap. In the present work we are interested prcmarcly in *changes in the band gaps* with structural parameters $\lambda$ (*e.g.*, bond length differences). We will therefore use the Slater exchange form to obtain the band gap for undistorted crystals ($\lambda = 0$), and verify that the derivative $\partial E_g/\partial\lambda$ does not depend strongly on the choice of exchange-correlation. We found this to be the case to within a very good approximation [2]. Figure 4 depicts the ground state electronic charge densities in a number of chalcopyrites. Figure 5 gives, for comparison with Figure 3, the calculated [7] band structure of two ternary pnictides.

Figures 3–5 show that: (i) $CuInSe_2$, like other chalcopyrites is a direct band gap material at $\Gamma$. (ii) The Cu3d states appear in the upper part of the valence band, hence these orbitals cannot be considered as chemically inert. In contrast, ternary pnictides [7] involve the deeper Zn3d band (Fig. 5) which is nearly chemically inert. (iii) The ground state charge density in chalcopyrites indicates the existence of two fundamen-

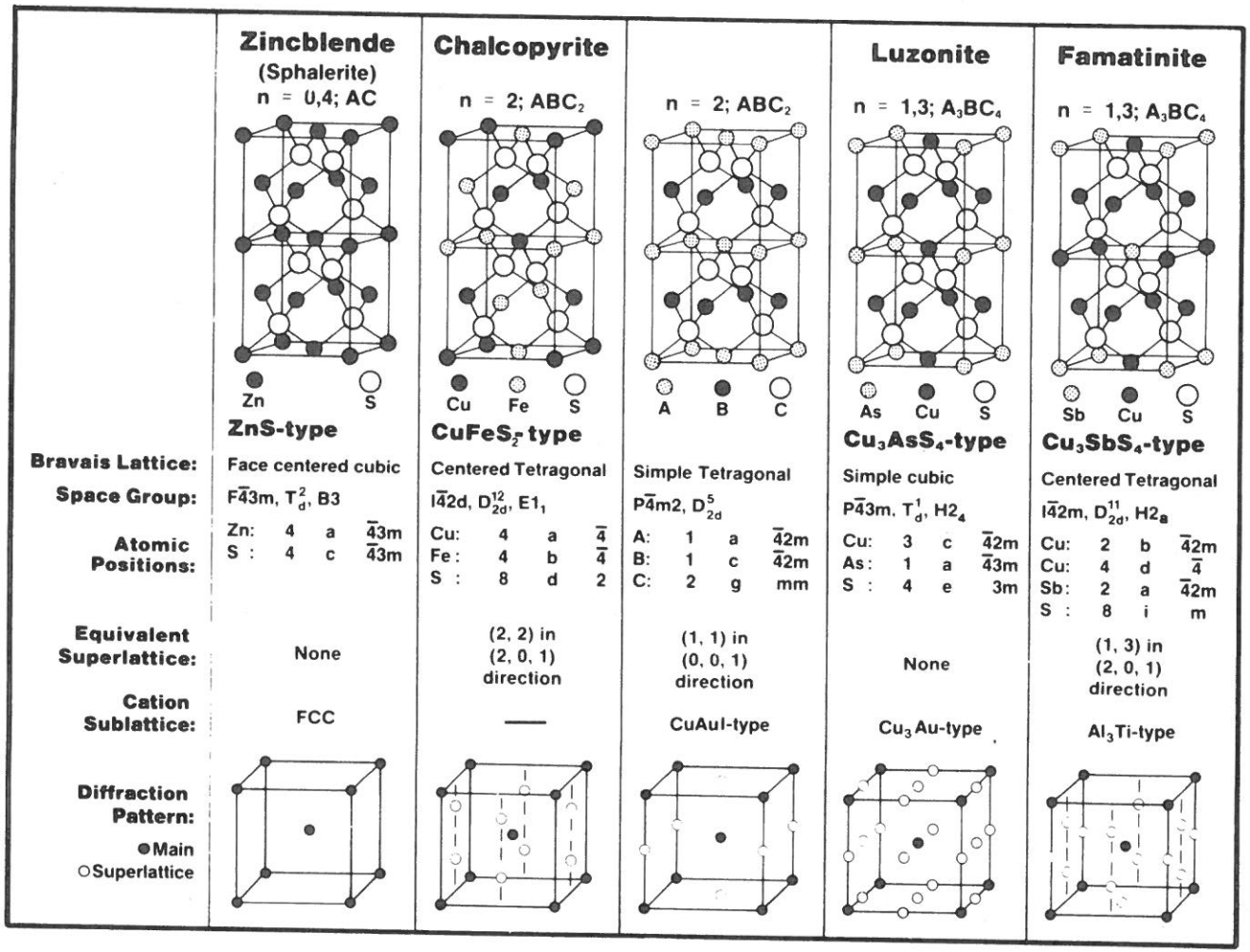


Figure 2. Five ordered crystal structures with the general formula $A_{4-n}B_nC_4$ which can be made from two fourfold coordinated $AC$ and $BC$ zincblende structures.

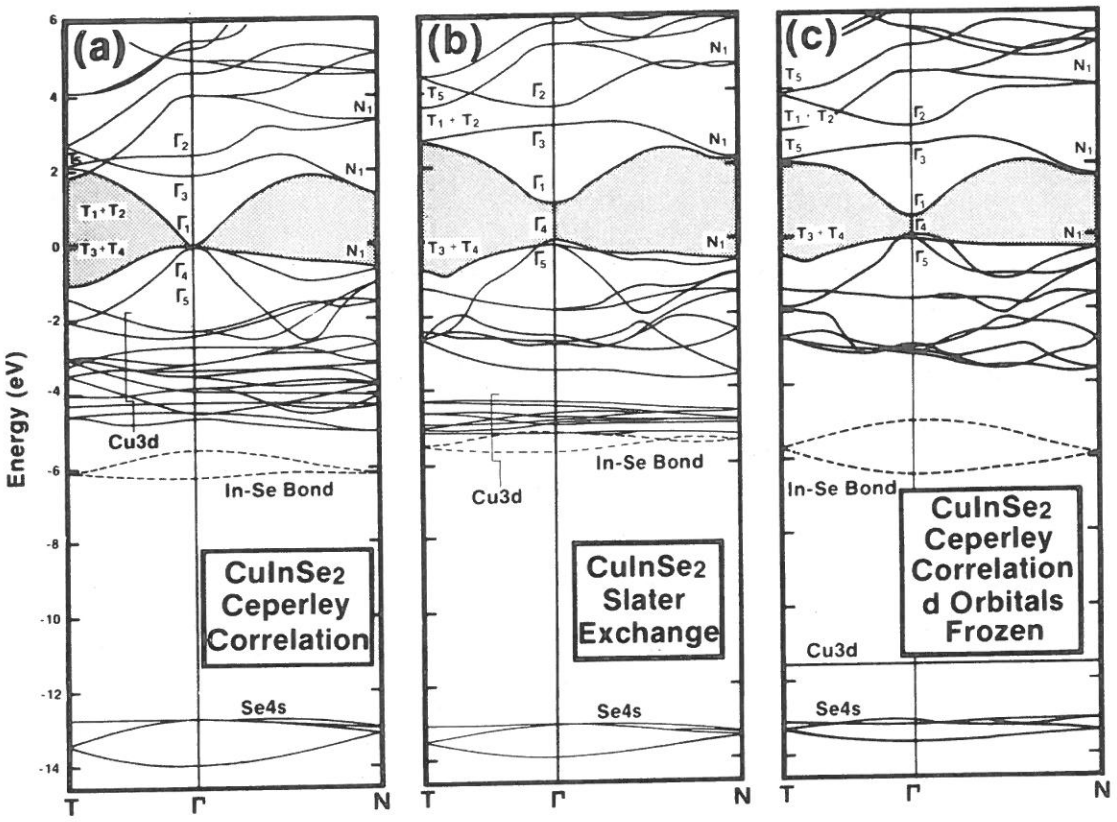


Figure 3. Calculated [2] band structure of $CuInSe_2$ in three different approximations.

tally different chemical bonds in the system: the Cu-anion bond, showing considerable bonding charge, (along with some ionic character), and the $B^{III}$-anion bond, showing essentially no bond formation. We will now use these conclusion to construct a systematic comparison of ternary with binary compounds.

## IV. A Stepwise Comparison of Binary and Ternary Systems

Our analysis of the atomic structure and band structure of the composite $A_{4-n}B_nC_4$ compounds suggests that the primary differences with their binary $AC$ and $BC$ compounds are as follows: (i) *Volume deformation:* the $A_{4-n}B_nC_4$ structures may have different unit cell volumes (per atom) than the $(4-n)AC+nBC$ structures. In general, the volume deformation can include changes both in the cubic lattice constant parameter $a$ and in the $c/a$ ratio. (ii) *Chemical electronegativity:* whereas in the composite structures the $A$-$C$ and $B$-$C$ bonds can interact and exchange charge (reflecting, e.g., their different electronegativities), these bonds obviously do not communicate in the isolated end-point materials. (iii) *Structural changes:* the composite structures can show bond alternation $R_{AC}^{(n)} \neq R_{BC}^{(n)}$, *i.e.*, they may be deformed relative to the ideal bonds $d_{AC}^0$ and $d_{BC}^0$. (iv) *p-d hybridization:* in the composite systems $A_{4-n}B_nC_4$ with $A=\text{Cu}$, there can be a distinct contribution to the bonding and band gaps from the active Cu3d orbits (c.f. Figs. 3 and 4) in contrast with the situation in Zn (or Ga) compounds (c.f. Fig. 5).

In trying to analyze the band gap anomalies in pseudobinary and real ternary systems, we could have used modern techniques of band theory [6] and calculate the band gaps of both ternary and binary systems and compare their difference with

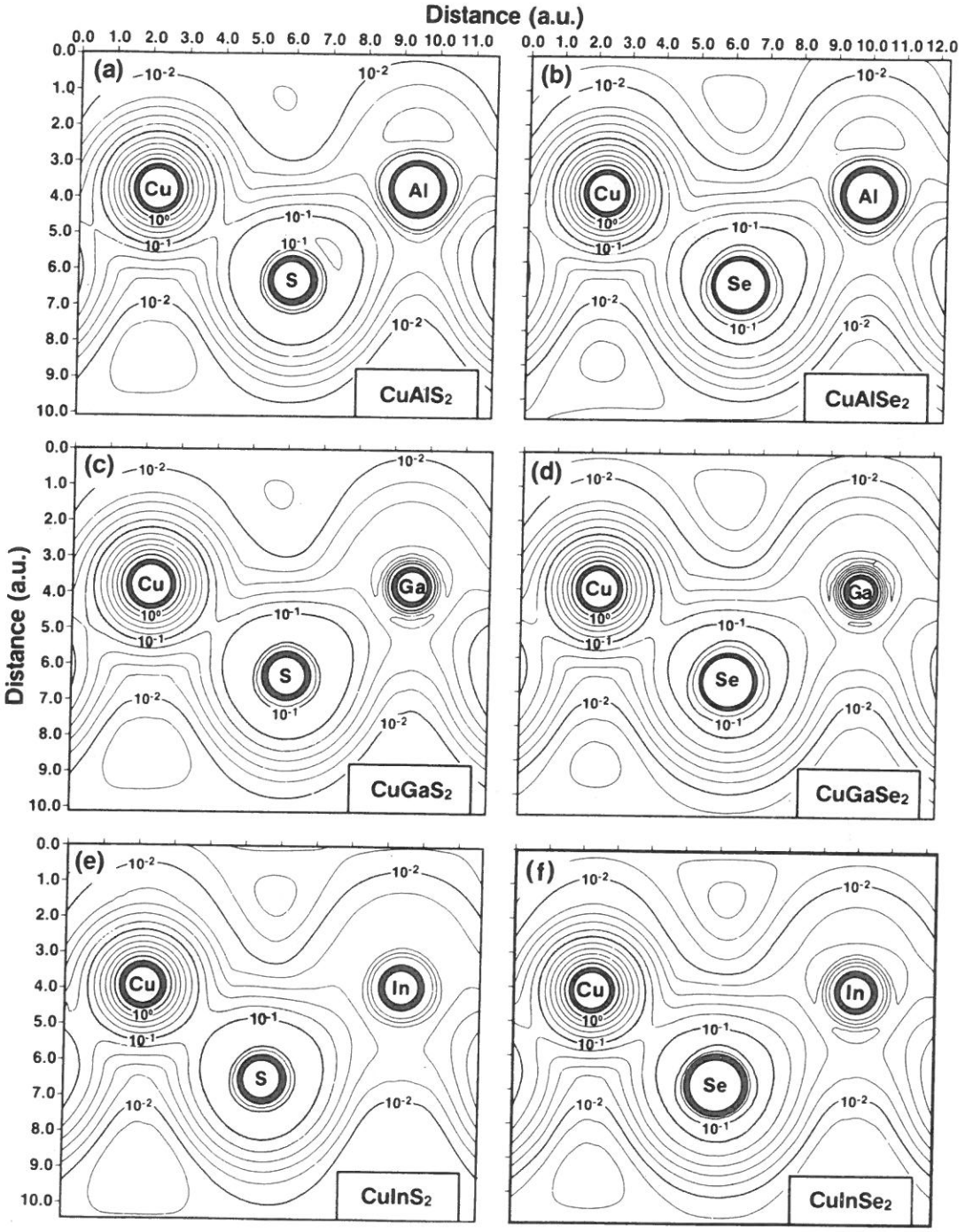


Figure 4. Calculated ground state electronic charge density in a number of ternary chalcopyrites.

experiment. This would merely reflect the extent to which such *ab-initio* computational techniques can mimic the data. However, our aim in this work is to gain an understanding of the physical and chemical mechanisms underlying structural and optical "anomalies" in ternary and pseudobinary systems. Therefore, we chose instead to break the general (formal) chemical reaction $(4-n)\bar{A}C + n\bar{B}C \rightarrow A_{4-n}B_nC_4$, where $\bar{A}=A$ and $\bar{B}=B$ for pseudobinary alloys like $x\mathrm{GaAs} + (1-x)\ \mathrm{InP} \rightarrow \mathrm{Ga}_x\mathrm{In}_{1-x}\mathrm{P}$, but $\bar{A}\neq A$ and $\bar{B}\neq B$ in real ternary systems, (where we compare 2ZnS with $CuGaS_2$), into artificial steps, corresponding to the differences (i) to (iv) enumerated above between

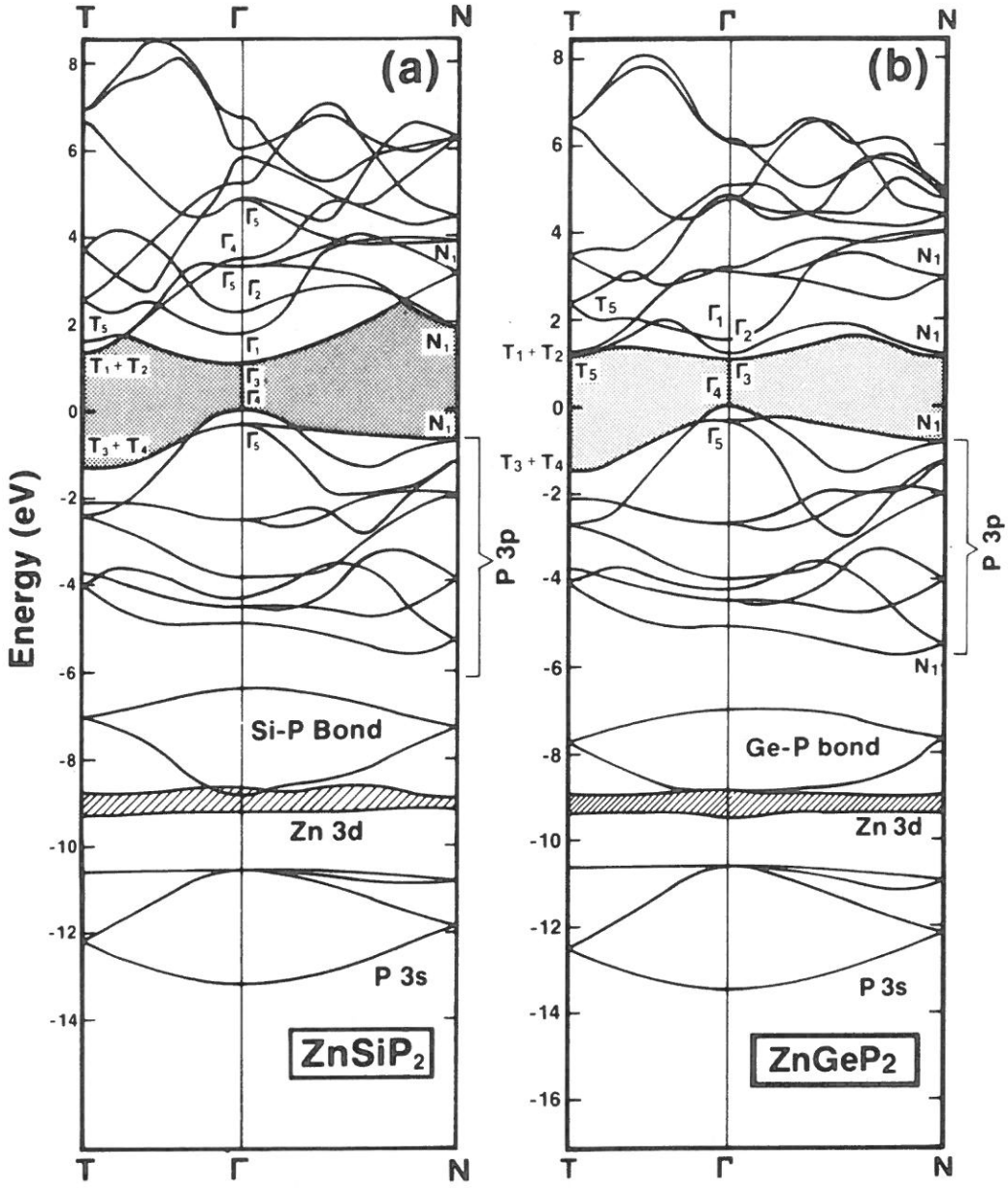


Figure 5. Calculated [2] band structure of two ternary pnictides.

the ternary and binary systems. What we hope to gain by this approach is a coherent picture of the factors affecting the optical (e.g., gaps) and structural (e.g., stability) properties of the ternary systems. In turn, we hope to use this understanding to design new materials. This will be discussed in Sec. VII and IX. We now proceed with a four-step (A to D) analysis of the evolution of ternary from binary systems.

### A. *Volume Deformation*

First, compress one structure (say $AC$, having an equilibrium lattice constant $a_{AC}^0$) and dilate the other (say, $BC$, having a lattice constant $a_{BC}^0$) so that both have the lattice constant $a_{eq}^{(n)}$ characteristic of the composite $A_{4-n}B_nC_4$ structure at equilibrium. The chemical reaction is

$$\left[(4-n)\bar{A}C,\, a_{AC}^0\right] + \left[n\bar{B}C,\, a_{BC}^0\right] \rightarrow \left[\bar{A}_{4-n}\,\bar{B}_n\,C_4,\, a_{eq}^{(n)}\right]. \tag{1a}$$

Had we adopted an empirical approach, we could have used the values of $a^0_{AC}$, $A^0_{BC}$ and $a^{(n)}_{eq}$ from experiment, together with the empirical equations-of-state of $AC$ and $BC$ (which depend on the known bulk modulii), and find the change in total energy attendant upon reaction (1a). We could, alternatively do this in a first-principle way, by computing $a^0_{AC}$, $a^0_{BC}$ and $a^{(n)}_{eq}$ from minimization of the total lattice energies of the three systems of Eq. (1a) and then find the change in the total energy corresponding to the reaction (1). We adopt this latter approach here. Denoting by $E$ either the total energy functional, or alternatively the band gap (for latter use), the change in energy upon volume deformation is

$$\Delta E^{VD} = (4-n)\left\{E[\bar{A}C,\, a^{(n)}_{eq}] - E[\bar{A}C,\, a^0_{AC}]\right\} + \left\{n\, E[\bar{B}C,\, a^{(n)}_{eq}] - E[\bar{B}C,\, a^0_{BC}]\right\} . \quad (1b)$$

Clearly, $\Delta E^{VD} > 0$, as we deform equilibrium structures.

### B. *Chemical Electronegativity*

In the second step, we let the "prepared" (i.e., volume-deformed) $\bar{A}C$ and $\bar{B}C$ systems combine to form the $A_{4-n}B_nC_4$ compound, however, without relaxing the bond lengths and angles beyond the values of the "prepared" systems. The chemical reaction can be written symbolically as

$$\left[(4-n)\bar{A}C,\, a^{(n)}_{eq}\right] + \left[n\bar{B}C,\, a^{(n)}_{eq}\right] \rightarrow \left[A_{4-n}B_nC_4,\, a^{(n)}_{eq},\, \text{undistorted, frozen } d\right] . \quad (2a)$$

For the pseudobinary case, we have $\bar{A} = A$ and $\bar{B} = B$, as discussed above. Also, since no chemically active $d$ electrons are involved in pseudobinaries (Column II and III) cations occurring in ZnS or GaAs have either no bound $d$ states, like Mg and Al, or deep $d$ states, like Zn and Ga, the notation "frozen $d$" is redundant. However, for ternary chalcopyrites, we compare in Eq. (2) 4 ZnS with $Cu_{4-n}Ga_nS_4$, hence $\bar{A} \neq A$ and $\bar{B} \neq B$. In this case, "frozen $d$" means that the right hand side of reaction (2) is calculated without taking into account the role of the Cu $d$ electrons, i.e., a "frozen $d$" calculation. This effect will be restored in step D below. The change in energy attendant upon reaction (2a) can be denoted as

$$\begin{aligned} \Delta E^{CE} \;=\; & E[A_{4-n}B_nC_4,\, a^{(n)}_{eq},\, \text{undistorted, frozen } d] \\ & -\; (4-n)\, E[\bar{A}C,\, a^{(n)}_{eq}] - n\, E[\bar{B}C,\, a^{(n)}_{eq}] . \end{aligned} \quad (2b)$$

In analogy, we define $\Delta\rho^{CE}(\underset{\sim}{r})$ as the corresponding difference in charge densities. In this step we allow therefore charge transfer [i.e., $\Delta\rho^{CE}(r) \neq 0$] between the $A$-$C$ and $B$-$C$ bonds: the charge will, most likely, be transferred from the less electronegative to the more electronegative bond, changing thereby the band gap and total energy. This step cannot be performed classically, and is neglected in non self consistent treatments.

### C. *Structural Change*

In the third step, we let the $A_{4-n}B_nC_4$ compound, with frozen $d$ orbitals and

undistorted bonds, to relax to its equilibrium bond lengths $R_{AC}^{(n)}$, $R_{BC}^{(n)}$ and angles. The reaction is

$$\left[A_{4-n}B_nC_4,\ a_{eq}^{(n)},\ \text{undistorted, frozen } d\right] \rightarrow \left[A_{4-n}B_nC_4,\ a_{eq}^{(n)},\ \text{equilibrated, frozen } d\right] \tag{3a}$$

with the corresponding change in energy

$$\Delta E^S = E[A_{4-n}B_nC_4,\ a_{eq}^{(n)},\ \text{equilibrated, frozen } d] - E[A_{4-n}B_nC_4,\ a_{eq}^{(n)},\ \text{undistorted, frozen } d]\ . \tag{3b}$$

The corresponding change in charge density is denoted $\Delta\rho^S(\underset{\sim}{r})$. In this calculation we let the bond lengths $R_{AC}^{(n)}$, $R_{BC}^{(n)}$ vary, to minimize the total energy of $A_{4-n}B_nC_4$. We do that under the restriction that the cations remain on the fcc lattice, as suggested by experiment [5].

Note that the energy $\Delta E^S$ could have been calculated semiclassically, by assuming some valence force field (VFF) which describes the strain energy of $A_{4-n}B_nC_4$ associated with bond-bending and bond-stretching. Such VFF are available, (e.g., the Keating model, c.f. Ref. 8 and references therein), however, they assume force constants of the *pure* $AC$ and $BC$ compounds. In other words, they neglect the interaction between the bonds through charge transfer. Denote the structural energy, analogous to (3b) obtained with such models as $\Delta E^{\text{VFF}}$. The difference between the full structural energy then $\Delta E^S$ of Eq. (3b) and $\Delta E^{\text{VFF}}$ is then defined as the polarization (pol) energy $\Delta E^{\text{pol}}$ which gives the *additional* structural relaxation due to deformation-induced charge transfer. We then have

$$\Delta E^S \equiv \Delta E^{\text{VFF}} + \Delta E^{\text{pol}}\ . \tag{3c}$$

### D. *p-h Hybridization*

In the final step we let the $A_{4-n}B_nC_4$ compound, with its relaxed geometry, to involve the $d$ orbitals, if available, in bonding. Computationally, this means that instead of doing a frozen-core calculation for the 3d states, we treat them dynamically as any other orbital. The reaction is

$$\left[A_{4-n}B_nC_4,\ a_{eq}^{(n)},\ \text{equilibrated, frozen } d\right] \rightarrow \left[A_{4-n}B_nC_4,\ a_{eq}^{(n)},\ \text{equilibrated, dynamic } d\right] \tag{4a}$$

and the corresponding change in energy is denoted $\Delta E^{pd}$.

### E. *The Net Reaction*

Adding up the four reactions (1a) to (4a), we have the net reaction

$$\left[(4-n)\bar{A}C,\ a_{AC}^0\right] + \left[\bar{B}C,\ a_{BC}^0\right] \rightarrow \left[A_{4-n}B_nC_4,\ a_{eq}^{(n)},\ \text{equilibrated, dynamic } d\right] . \quad (5a)$$

Calculation of the optical and structural properties of both sides of this reaction will provide all information which is necessary to deduce optical bowing and structural stability parameters. Using our "Born-Haber"-like cycle, the change in energy attendant upon this reaction is

$$\Delta E_{eq}^{(n)} = (\Delta E^{VD} + \Delta E^{\text{VFF}}) + (\Delta E^{\text{pol}} + \Delta E^{CE} + \Delta E^{pd}) , \quad (5b)$$

or

$$\Delta E_{eq}^{(n)} \equiv \Delta E^{\text{strain}} + \Delta E^{\text{chem}} ,$$

where we have denoted the first two terms, which can be computed classically as "strain energy," while the last three terms reflect "chemical energy." Note that $\Delta E^{\text{strain}}$ is positive-definite since straining the equilibrium $\bar{A}C$ and $\bar{B}C$ systems can never lower their energy. If $E$ in Eqs. (1–5) were to denote the total energy per mole relative to separated atoms, then the condition

$$E[A_{4-n}B_nC_4,\ a_{eq}^{(n)},\ \text{equilibrated, dynamic } d] < 0 \quad (5c)$$

implies that the $A_{4-n}B_nC_4$ system is stable towards dissociation to atoms (i.e., positive cohesive energy), whereas the condition

$$\Delta E_{eq}^{(n)} < 0 , \quad (5d)$$

implies that $A_{4-n}B_nC_4$ is also stable against disproportionation into its endpoint compounds $\bar{A}C$ and $\bar{B}C$. If $E$ were to denote band gaps, then $\Delta E_{eq}^{(n)} < 0$ implies positive optical bowing.

## V. *Other Approaches*

Our discussion and definitions of Section IV allows us to discuss various approximations used in the past. Before proceeding with our own results, we briefly discuss these other approaches.

(i) *In the Virtual Crystal Approximation* (VCA) [9] one assumes that the individuality of the $\bar{A}$ and $\bar{B}$ atoms is lost in the alloy, and replaced by a fictitious (nonexisting) "average" atom $\langle\bar{A}\bar{B}\rangle$. The bond lengths between $C$ and each of the $\langle\bar{A}\bar{B}\rangle$ species is assumed therefore to be constant. Furthermore, since in the pure $AC$ system the bond length $d_{AC}^0$ is related *geometrically* to the lattice constant $a_{AC}^0$ (i.e., in zincblende structures $d_{AC}^0 = \frac{\sqrt{3}}{4} a_{AC}^0$), it was assumed in VCA [9] that this continues to be the case in the alloy, where $R_{AC}^{(n)} = R_{BC}^{(n)} = \frac{\sqrt{3}}{4} a_{eq}^{(n)}$. Hence, in the VCA

$$\Delta E^{\text{VFF}} = \Delta E^{pd} = \Delta E^{\text{pol}} = \Delta E^{CE} \equiv 0 . \quad (6)$$

(ii) *In strain-minimizing models* [10–11], one neglects the chemical energy and

deduces the equilibrium structure from the minimization of the positive-definite force field $\Delta E^{VD} + \Delta E^{VFF}$. Hence, it is assumed that $\Delta E^{chem} \equiv 0$. Whereas, such approaches automatically accept the instability of $A_{4-n}B_nC_4$ towards disproportionation (i.e., $\Delta E_{eq}^{(n)} > 0$), surprisingly they predict the correct *geometry* of the compound. Examples are given in Figures 6 and 7 which compare the calculated lattice constant and anion-displacement parameters of chalcopyrites and pnictides with the observed values. Here, the calculation [2] has been done by the "Conservation of Tetrahedral Bonds" (CTB) model, which assumes, following the classical ideas of Bragg and Pauling, that bond lengths are approximately conserved quantities in different bonding environments. A similar conclusion is evident from Figure 8, where we present the percent bond length change around an isovalent impurity in a semiconductor [8]. This has been calculated by minimizing the valence-force-field of Keating for impurities in host crystals, where the impurity-host force constants is taken from a prototype host crystal (e.g., for a In impurity in GaAs, we describe the In-As interactions by a VFF of bulk InAs, and the Ga-As interactions are described by a VFF of bulk GaAs). These results suggest, surprisingly, that whereas the value of the function $\Delta E_{eq}^{(n)}$ at equilibrium may be affected by $\Delta E^{chem}$, the *position* of the equilibrium is not. Classical ideas of bond conservation and transferable force fields may hence be adequate for geometries, but not for energies.

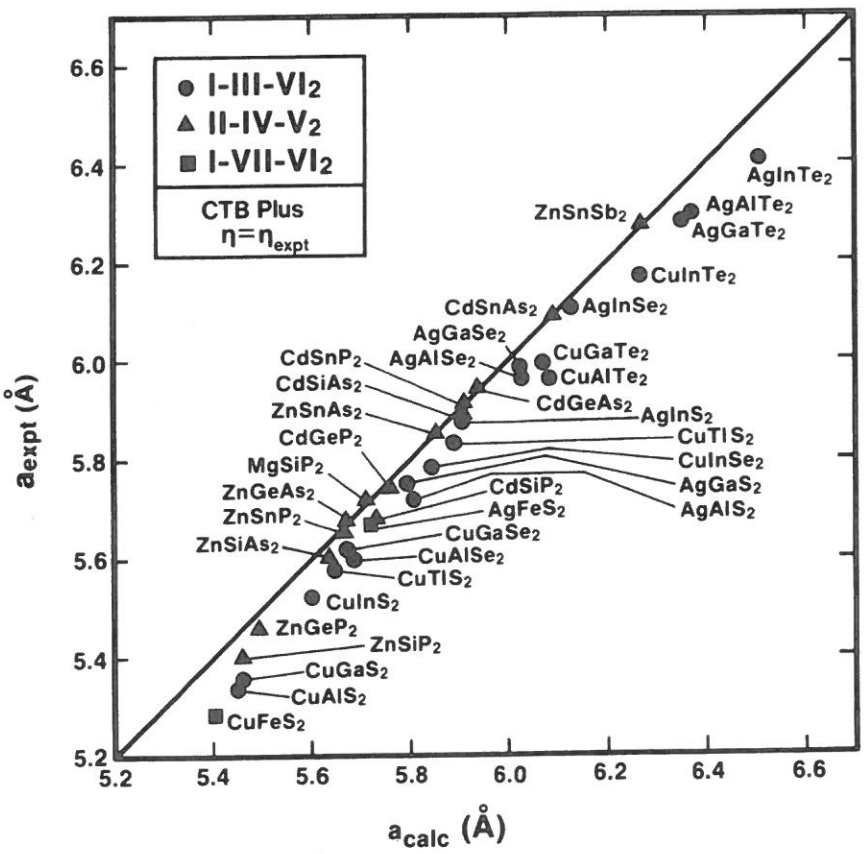


Figure 6. Calculated [2] and observed (Refs. given in 2) lattice constants of ternary semiconductors. The calculation uses the "Conservation of Tetrahedral Bonds" (CTB) model, where it is assumed that the ternary lattice assumes the form which minimizes the strain that would arise from bond lengths being different from their ideal binary values. The only input are the bond lengths in *binary* zincblende compounds.

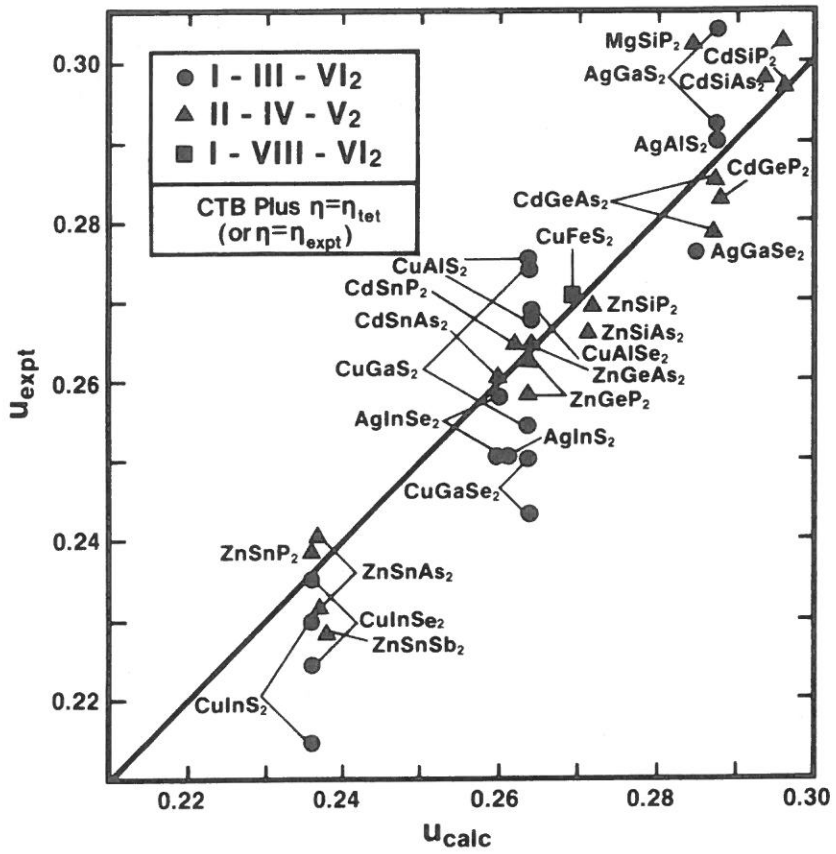


Figure 7. Calculated [2] and observed anion displacement parameters in ternary semiconductors. See caption to Figure 6.

(iii) *Models for alloy stability:* Our decomposition of the energy change in Eqs. (1)–(5) can also be used to discuss contemporary approaches to *alloy stability*. Under normal preparation conditions, semiconductor alloys are "quenched" from high-temperatures, leaving one with randomly disordered alloys. For all III–V alloys, (for which data exists) the change in energy for the reaction

$$\left[(4-n)\bar{A}C,\, a^0_{AC}\right] + \left[n\bar{B}C,\, a^0_{BC}\right] \rightarrow \left[\bar{A}_{4-n}\bar{B}_nC_4,\, \text{Random}\right] \tag{7a}$$

*i.e.*,

$$\Delta H_D = E[\bar{A}_{4-n}\bar{B}_nC_4,\, \text{Random}] - (n-4)\, E[\bar{A}C\; a^0_{AC}] - n\, E[\bar{B}C\; a^0_{BC}] \tag{7b}$$

was found [11] to be *positive* for randomly disordered ($D$) alloys (the change in enthalpy $\Delta H_D$ is very close to the change in internal energy since PV is negligible at 1 atmosphere). This had led many workers to tacitly assume that since the formation energy of a *random* system [Eq. (7)] is positive, the *ordered* system [Eq. (5)] is probably also unstable towards disproportionation. For instance, in Stringfellow's model [11] it is postulated that the enthalpy $H$ of *any* phase, ordered or disordered, is a convex function of its lattice parameter, i.e., $H = -\frac{K}{a^p}$, (where $K$ is an empirical constant and $p > 0$). Hence, any phase with a lattice parameter intermediate between those of its constituent compounds will have $\Delta H > 0$. Similarly, in Van Vechten's model [12], positive optical bowing accompanying compound formation is interpreted as a

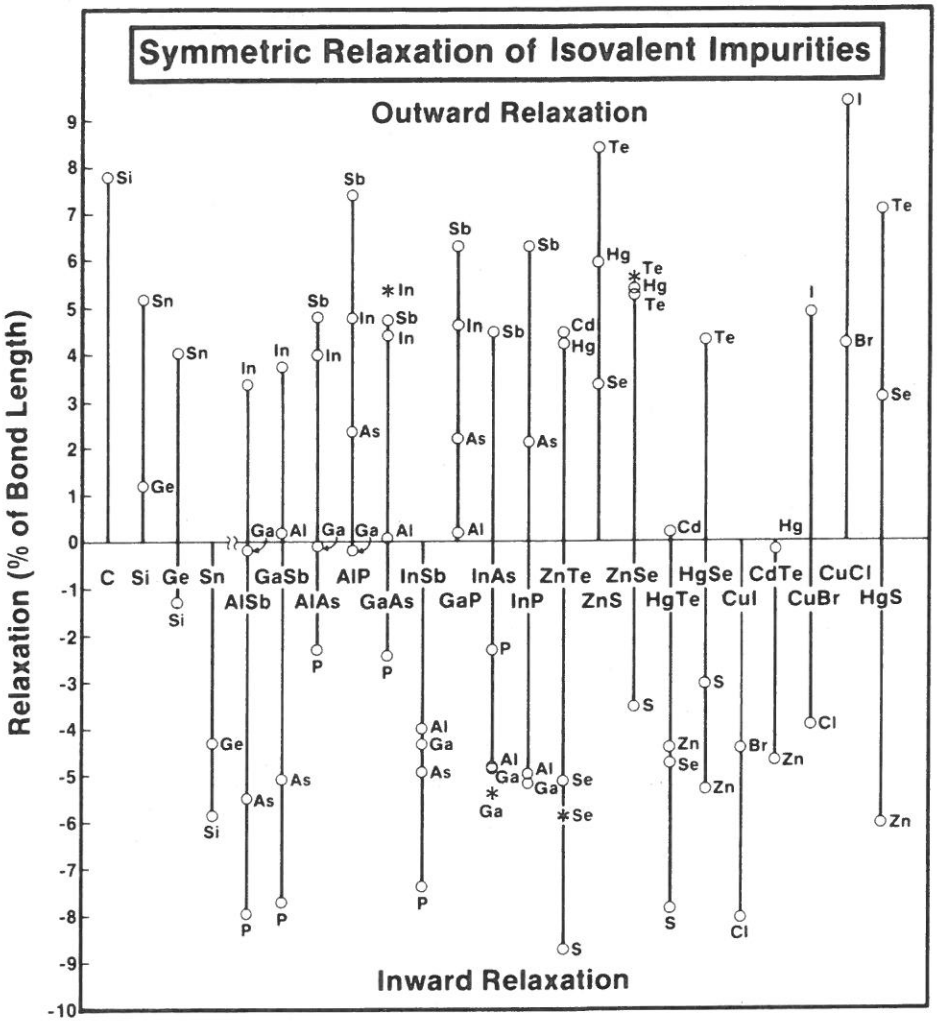


Figure 8. Calculated (method of Ref. 8) percent changes in the bond lengths around isovalent impurities (open circles) in semiconductors (indicated on the $X$ axis). Asterisks denote observed values (Ref. 8 and references therein).

(destabilizing) upward shift of the valence band energies, leading to $\Delta H > 0$ for either ordered or disordered compounds whose gaps are reduced relative to their average. All strain-minimizing models [10] necessarily lead to $\Delta H > 0$, as the strain energy is positive-definite. Our analysis suggests that these conclusions, based upon considerations of *strain energy alone*, are misleading. We will show (c.f. Sec. IX) that whereas for random systems $\Delta H_D > 0$, ordered compounds can nevertheless be stable, i.e., $\Delta E_{eq}^{(n)} < 0$ due to the dominance of stabilizing chemical effects over the destabilizing strain effects.

## VI. Band Gap Anomaly in Ternary Chalcopyrites

We have calculated the band gap anomaly in ternary chalcopyrites along the conceptual decomposition outlined in Sec. IV. Our analysis shows that most of the change in band gaps arises from the structural energy $\Delta E^S$ and the pd hybridization energy $\Delta E^{pd}$. Figure 3 compares the band structure of $CuInSe_2$ calculated with dynamic (3a) and frozen (3c) Cu 3d orbitals. When the Cu 3d orbitals are excluded from

bonding, the Cu 3d band separates in energy from the main valence band, and drops to $\sim -12$ eV. The bonding-antibonding repulsion diminishes, resulting in an *increase* in the band gap. We find $\Delta E^{pd} = 0.7$ eV. Figure 9 depicts the band structure of $CuInSe_2$ and $CuAlS_2$ as a function of the anion displacement parameter $u$. When $u \equiv \frac{1}{4}$, the two bond lengths (e.g., $R_{Cu\text{-}Se}$ and $R_{In\text{-}Se}$) are equal. The experimental value for $CuInSe_2$ is $u = 0.224$. We see from Figure 9 that when $u$ changes from $\frac{1}{4}$ (equal bonds) to its (smaller) experimental value, the band gap *decreases*. We hence find $\Delta E^S = 0.50$ eV. This effect can be thought of as an ionicity effect, as depicted in Figure 10. We see that for the unequal bond arrangement (e.g., for $u = 0.2$) the system exhibits covalency in the Cu-Se bond, whereas for the equal-bond arrangement this bond charge disengages, forming a more ionic bond with its attendant larger band gap.

Table II summarizes some of our results for the band gap anomaly in ternary chalcopyrites. We show the observed anomaly $\Delta E_g^{obs}$ as well as the observed anion displacement parameter $u$. The calculated structural contribution $\Delta E^S$ can be either positive (when $u < \frac{1}{4}$), or negative (when $u > \frac{1}{4}$). We then inspect all contributions to $\Delta E_g$ other than the structural part, i.e.,

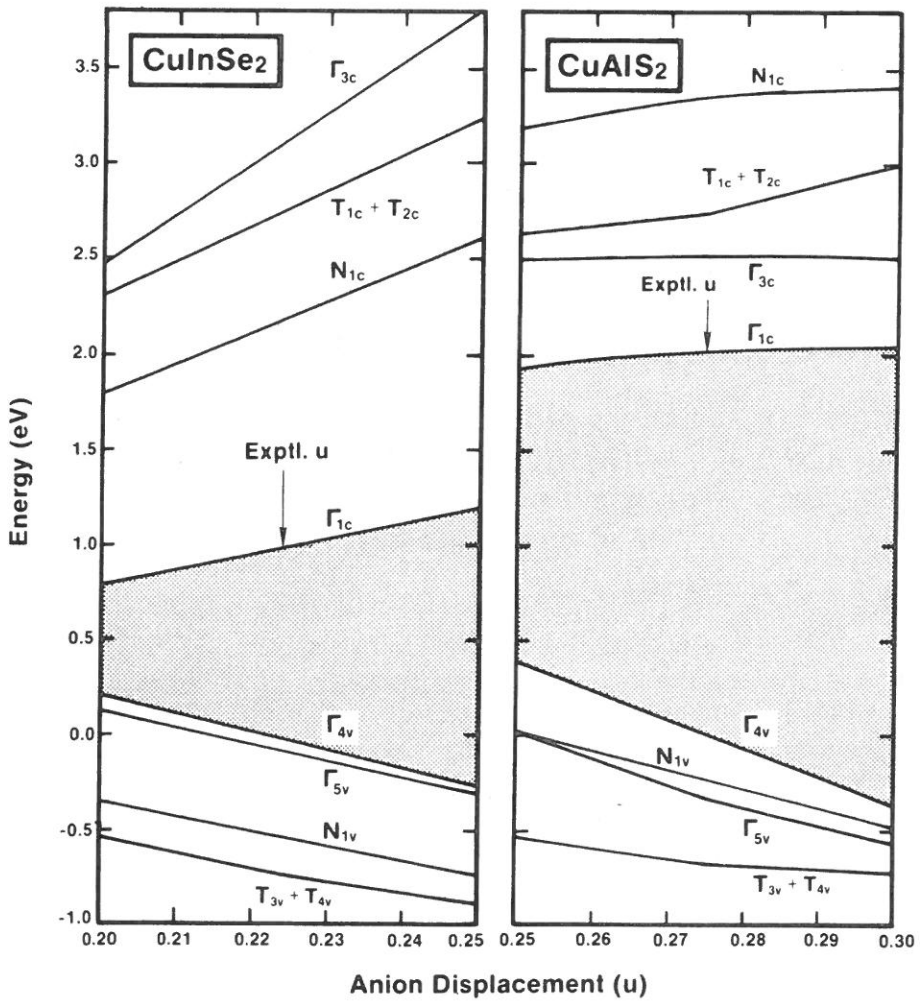


Figure 9. Band energies of two chalcopyrites, as a function of the anion displacement parameter $u$. For $u = 1/4$, the two bond lengths are equal.

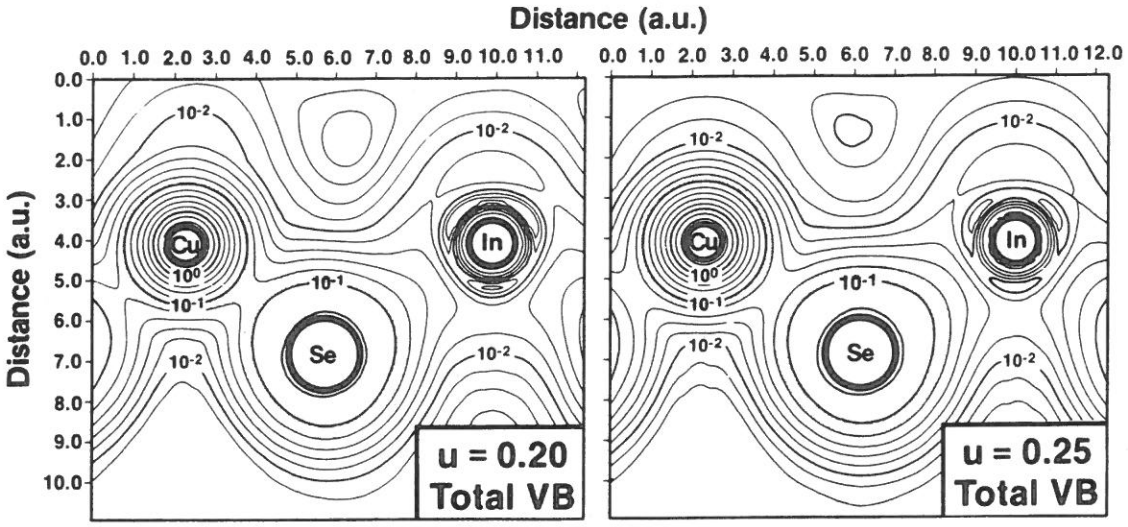


Figure 10. Comparison of the total valence band (VB) change densities for an equal-bond $CuInSe_2$ structure ($u = 0.25$, note ionic separation of charge) with that of a bond-alternating structure ($u = 0.20$, note the covalent bond charge).

$$\Delta E_g - \Delta E_g^S = \Delta E_g^{VD} + \Delta E_g^{CE} + \Delta E_g^{pd} .$$

We see from Table II that $\Delta E^{pd}$ accounts for most of the nonstructural part of the band gap anomaly $\Delta E_g$. This analysis establishes the structural bond relaxation and p-d hybridization as the souces of the band gap anomaly in ternary chalcopyrites. More details are given elsewhere [2,7].

## VII. Predictions of Some New Chalcopyrites

Having understood the factors affecting the band gaps of ternary chacopyrites in terms of chemical (i.e., p-d hybridization) and structural (i.e., bond alternation) effects, and the way the structural parameters are dictated by atomic sizes (Figs. 6 and 7), we are now in a position to predict gaps and structural parameters for *hitherto*

TABLE II. Decomposition of the observed band gap anomaly (*c.f.* Table I) into its calculated structural component $\Delta E_g^S$ and nonstructural (*NS*) component $\Delta E_g^{NS}$. The major contribution to the latter is seen to arise from the p-d hybridization effect ($\Delta E_g^{pd}$), calculated here for the two end compounds. For comparison, we give the value of the experimental anion displacement parameters $u$.

| Material | $\Delta E_g^{observed}$ | u | $\Delta E_g^S$ | $\Delta E_g^{chem} \equiv \Delta E_g^{obs} - \Delta E_g^S$ | $\Delta E_g^{pd}$ |
|---|---|---|---|---|---|
| $CuInSe_2$ | 1.3 | 0.224 | 0.5 | 0.70 | 0.72 |
| $CuInS_2$ | 1.6 | 0.214 | 0.7 | 0.9 | --- |
| $CuGaSe_2$ | 1.0 | 0.25 | 0.0 | 1.0 | --- |
| $CuAlSe_2$ | 1.4 | 0.269 | -0.38 | 1.81 | --- |
| $CuGaS_2$ | 1.4 | 0.275 | -0.50 | 1.87 | --- |
| $CuAlS_2$ | 2.4 | 0.275 | -0.50 | 2.90 | 2.98 |

TABLE III. Predicted structural parameters and estimated band gaps ($E_g$) for 22 possible chalcopyrite-structure semiconductors. The symbol PD in the bandgap column indicates compounds most likely to have pseudodirect lowest gaps.

| Compound | a (Å) | u | η | $E_g$ (eV) |
|---|---|---|---|---|
| $ZnSiSb_2$ | 6.077 | .270 | .961 | 0.9 |
| $ZnGeSb_2$ | 6.111 | .263 | .975 | 0.5 |
| $CdSiSb_2$ | 6.344 | .291 | .921 | 0.8 |
| $CdGeSb_2$ | 6.383 | .285 | .933 | 0.2 |
| $MgGeP_2$ | 5.656 | .277 | .947 | 2.1 (PD) |
| $MgSnP_2$ | 5.774 | .250 | 1.000 | 1.8 |
| $MgSiAs_2$ | 5.804 | .284 | .935 | 2.0 (PD) |
| $MgGeAs_2$ | 5.841 | .276 | .949 | 1.6 |
| $MgSnAs_2$ | 5.958 | .250 | 1.000 | 1.2 |
| $MgSiSb_2$ | 6.221 | .281 | .939 | 1.4 |
| $MgGeSb_2$ | 6.258 | .275 | .952 | 0.9 |
| $MgSnSb_2$ | 6.374 | .250 | 1.000 | 0.6 |
| $HgSiP_2$ | 5.740 | .296 | .913 | 1.6 |
| $HgGeP_2$ | 5.780 | .288 | .927 | 1.2 |
| $HgSnP_2$ | 5.909 | .262 | .977 | 0.8 |
| $HgSiAs_2$ | 5.926 | .294 | .916 | 0.7 |
| $HgGeAs_2$ | 5.966 | .287 | .929 | 0.2 |
| $CuTlTe_2$ | 6.299 | .233 | 1.034 | 0.9 |
| $AgTlS_2$ | 5.882 | .257 | .986 | 1.1 |
| $AgTlSe_2$ | 6.113 | .257 | .986 | 0.7. |
| $AgTlTe_2$ | 6.529 | .257 | .987 | 0.6 |
| $BeCN_2$ | 3.847 | .313 | .883 | 8.2 (PD) |

*unknown chalcopyrite structures*. Table III provides a list of predictions of such new compounds with their anticipated band gaps and lattice parameters. This list reveals a number of new materials of potential significance in device applications. Synthesis of some of these materials is underway in our laboratory.

## VIII. Optical Bowing in Semiconductor Alloys

We can carry out a similar analysis for the band gap anomaly in semiconductor alloys (i.e., optical bowing). For example, Figure 11 depicts the variation in the structural part of the band gap $\Delta E_g^S$ of a true ternary ($CuInSe_2$) and a pseudobinary ($InGaP_2$) with the bond alternation parameter. We see that the band gap in both system diminishes with bond alternation. This analysis hence reveals that the structural effect is common to both systems: the difference is largely quantitative, as chalcopyrites show a larger

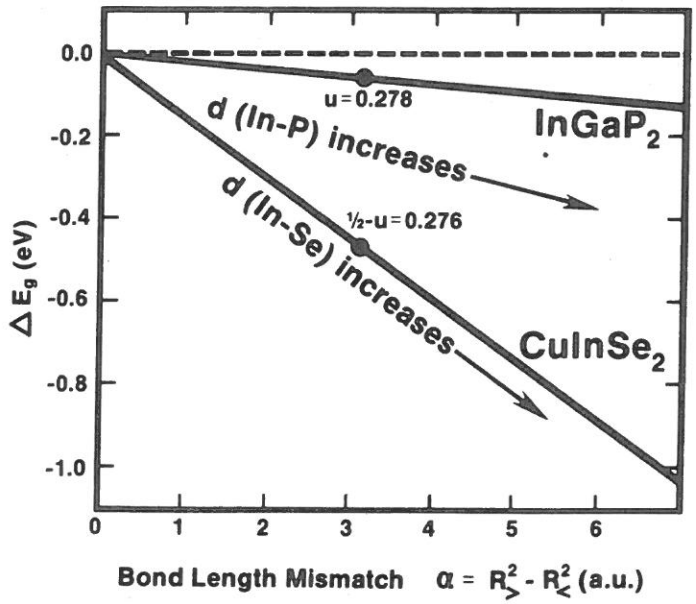


Figure 11. Comparison of the variations in the structural part $\Delta E_g^S$ of the band gap as a function of the mismatch in bond lengths for a true ternary crystal ($CuInSe_2$) with that of an hypotetically ordered pseudobinary crystal ($InGaP_2$).

sensitivity $\partial \Delta E_g^S / \partial u$ to bond alternation relative to pseudobinaries. However, bond alternation is a decisive factor in establishing optical bowing in pseudobinary alloys, since the deviation of their gaps from those of the parent materials is usually very small [1].

Table IV summarizes some of our calculated results for the optical bowing parameters of pseudobinary alloys. We see that systems with a large atom-size-mismatch (e.g., $In_xGa_{1-x}P$,$ZnSe_xTe_{1-x}$) show a substantial structural component to the bowing, whereas systems with nearly equal atomic sizes (e.g., $Ga_xAl_{1-x}As$) have small bowing parameters. Notice that our analysis of the optical bowing assumed *ordered models* for the alloy. We hence interpret the difference between the observed and calculated bowing parameters in Table IV as being due to disorder effects. This analysis hence suggests that disorder may be the prevailing physical phenomena in alloys with small size mismatch, whereas in alloys with substantial size and electronegativity mismatch, *local order effects* are dominant. This leads us to suspect that some alloys could order crystalographically if grown appropriately. We discuss this point next.

TABLE IV. Structural (*S*), nonstructural (*NS*) and experimental optical bowing parameters of some pseudobinary systems.

| System | $b^{NS}$ | $b^{S}$ | $b^{tot}$ | $b^{exp}$ |
|---|---|---|---|---|
| $InGaP_2$ | 0.25 | 0.17 | 0.42 | ~0.5 |
| $SeTeZn_2$ | 0.40 | 0.93 | 1.33 | ~1.3 |
| $GaAlAs_2$ | -0.01 | 0.00 | -0.01 | <0.1 |

## IX. Ordering in Pseudobinary Systems

We have calculated the ordering energy $\Delta E_{eq}^{(n)}$ of Eq. (5) for a model of a pseudobinary crystal $In_xGa_{1-x}P$. *Here, E takes the role of the total energy relative to separated atoms*. We neglect the $\Delta E^{pd}$ part, as In, Ga and P do not have chemically active *d* states. We use the pseudopotential total energy method [13] within a self-consistent plane-wave basis, describing exchange and correlation effects within the density functional formalism.

For the end-point crystals GaP ($n=0$) and InP ($n=4$), we find [14] calculated equilibrium lattice constants $a_{GaP}^0$ and $a_{InP}^0$ that are within 1.5% of experiments, like in other recent calculations [15]. We find InP to have *weaker* bonds than GaP (the cohesive energy $-E_{InP}[a_{InP}^0]$ is smaller by 4 kcal/mol than that of GaP) and a *larger* degree of ionicity: its maximum charge density $\rho_{max}=32.5$ e/cell is both larger than that of GaP ($\rho_{max}=31$ e/cell, the experimental value is [16] $35\pm3$ e/cell) and is drawn closer to the *P* site. For the intermediate compounds $n = 1,2,3$, i.e., $Ga_3InP_4$, $Ga_2In_2P_4$ and $GaIn_3P_4$, respectively, we find equilibrium lattice constants $a_{eq}^{(n)}$ that are within 0.5% of the calculated composition-weighted average values $\bar{a}(n)\equiv\frac{4-n}{4}a_{GaP}^0+\frac{n}{4}a_{InP}^0$, confirming thereby quantum mechanically Vegard's rule [$a_{eq}^{(n)}=\bar{a}(n)$] for the ordered compounds. However, bond lengths do not average as lattice constants do [i.e. $\Delta_{AC}\neq(x-1)(d_{AC}^0-d_{BC}^0)$]. We find very small equilibrium deformations $\Delta^{(n)}\leqslant0.01$Å (solid circles in Fig. 12), indicating that throughout the composition range the bond lengths tend to stay very close to their values in the parent crystals. These results parallel the observed and calculated anion displacements in real Chalcopyrites [2] and reflect the classical idea by Bragg and Pauling that bond radii are approximately conserved quantities in different chemical environments [$\Delta^{(n)}\cong0$]. What is new, however, in the present quantum mechanical result relative to classical theory is that we predict the intermediate compounds to be not only stable relative to dissociation into free atoms i.e. ($E_{A_{4-n}B_nC_4}<0$), but to also be stable towards disproportionation into its constituent binary compounds [i.e. $\Delta E_{eq}^{(n)}<0$, whereas classical additivity of bond energies wou give $\Delta E^{(n)}\equiv0$ in Eq. (5b)]. We illustrate the mechanisms leading to this stability by considering the process $(4-n)AC+nBC\rightarrow A_{4-n}B_nC_4$ in three steps, as discussed in Section III A–C. First, compress $a_{InP}^0$ and dilate $a_{GaP}^0$ to the equilibrium lattice $a_{eq}^{(n)}$ of the intermediate compound. For $n = 2$ we find that the energy is raised by the volume deformation (*VD*) contribution $\Delta E^{VD} = 0.87$ kcal/mol due to this uniform elastic strain. This is the only contribution considered in virtual crystal models [10] which grossly overestimate $\Delta E^{(n)}$. Second, bring together $4-n$ *AC* cells and *n BC* cells, both prepared at $a_{eq}^{(n)}$, to form the crystal $A_{4-n}B_nC_4$, without relaxing the internal bond lengths and angles [*i.e.* $R_{AC}^{(n)}=R_{BC}^{(n)}=\frac{\sqrt{3}}{4}a_{eq}^{(n)}$] to their equilibrium values. The energy change is $\Delta E^{CE}$. Figure 13(a) displays the corresponding difference [c.f. Eq. (2b)] in charge densities $\Delta\rho^{CE}(\vec{r}) = \rho[GaInP_2, a_{eq}^{(2)}, \text{undistorted}] - 2\rho[GaP, a_{eq}^{(2)}] - 2\rho[InP, a_{eq}^{(2)}]$. It shows that charge flows from the less ionic Ga-P bond to the more ionic (but weaker) In-P bond, as Phillips' ionicity ($f_{GaP}=0.327$, $f_{InP}=0.421$) would suggest. We calculate a small positive $\Delta E^{CE} = 0.85$ kcal/mol, reflecting accumulation of extra charge on the weaker bond. (In general $\Delta E^{CE}$ could also be negative, if the more ionic bond, e.g., Ga-P, is stabler than the less ionic bond, e.g., Ga-As). In the final step we relax the

internal bond lengths and angles to achieve equilibrium at $\Delta_{eq}^{(n)}$, involving structural ($S$) energy change of $\Delta E^S = -3.2$ kcal/mol which stabilizes the system. Had we done this last step semiclassically by minimizing the bond bending and stretching energies, using force constants of the *noninteracting* $AC$ and $BC$ compounds (i.e., the valence force field, VFF approach) we would have obtained only a small energy stabilization of $\Delta E^{\text{VFF}} = -0.7$ kcal/mol. This would have neglected deformation-induced charge transfer. Figure 13(b) shows the self-consistently calculated deformation-induced charge transfer $\Delta\rho^S(\vec{r}) = \rho[\text{GaInP}_2, a_{eq}^{(2)}, \text{equilibrated}] - \rho[\text{GaInP}_2, a_{eq}^{(2)}, \text{undistorted}]$ and Figure 13c shows similarly $\Delta\rho^S(\vec{r})$ for $GaIn_3P_4$. They indicate substantial charge redistributions: the stabler Ga-P bond (with a deep Ga pseudopotential) acquire *more* charge than it lost in the previous step to the In-P bond (with the shall lower In pseudopotential). The corresponding polarization (pol) energy is $\Delta E^{\text{pol}} \equiv \Delta E^S - \Delta E^{\text{VFF}} = -2.5$ kcal/mol for $n = 2$ and constitutes the main driving force for stability. The total excess energy of the ordered compound is $\Delta E_0 = \Delta E_{eq}^{(n)} = (\Delta E^{VD} + \Delta E^{\text{VFF}}) + (\Delta E^{CE} + \Delta E^{\text{pol}})$. We find $\Delta E_{eq}^{(2)} = -1.48$ kcal/mol for the Chalcopyrite. The ordered simple tetragonal structure is only 0.1 kcal/mol less stable; similarly the Luzonite and Famatinite structures are also close to one another in stability.

A few observations are in order. First, the closeness of the ordered phase energies $\Delta E_0$ for these polytype pairs suggests that all are likely to form kinetically at growth temperatures, but the choice of growth (i.e., substrate) orientation might discriminate them: the Chalcopyrite is a (2,2) superlattice in the (2,1,0) direction whereas the simple tetragonal CuAu-I-like structure is a (1,1) superlattice in the (1,0,0) direction. We hence predict these particular superlattices to be *intrinsically* (not accidentally) stable against alloy formation below an ordering temperature $T_0 = (\Delta H_D + \Delta E_0)/\Delta S_D$. Second, these structures can be identified by their fingerprint diffraction beams. They

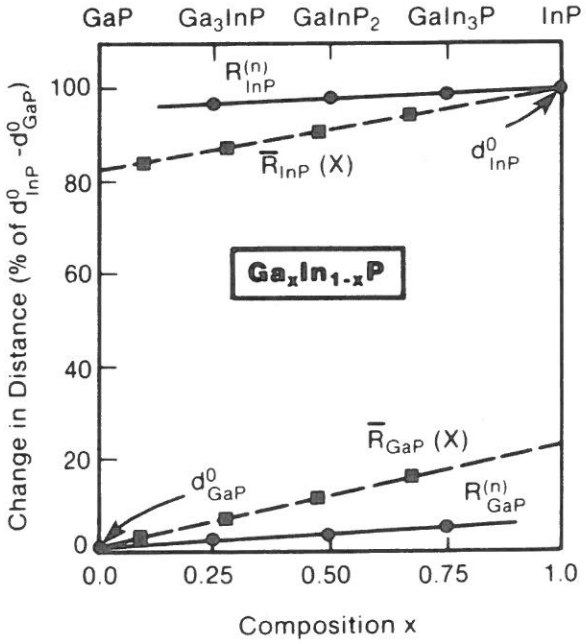


Figure 12. Percent charge (in units of $d_{\text{InP}}^0 - d_{\text{GaP}}^0$) of the near-neighbor bond lengths in ordered phases (0) and in random alloys ( ).

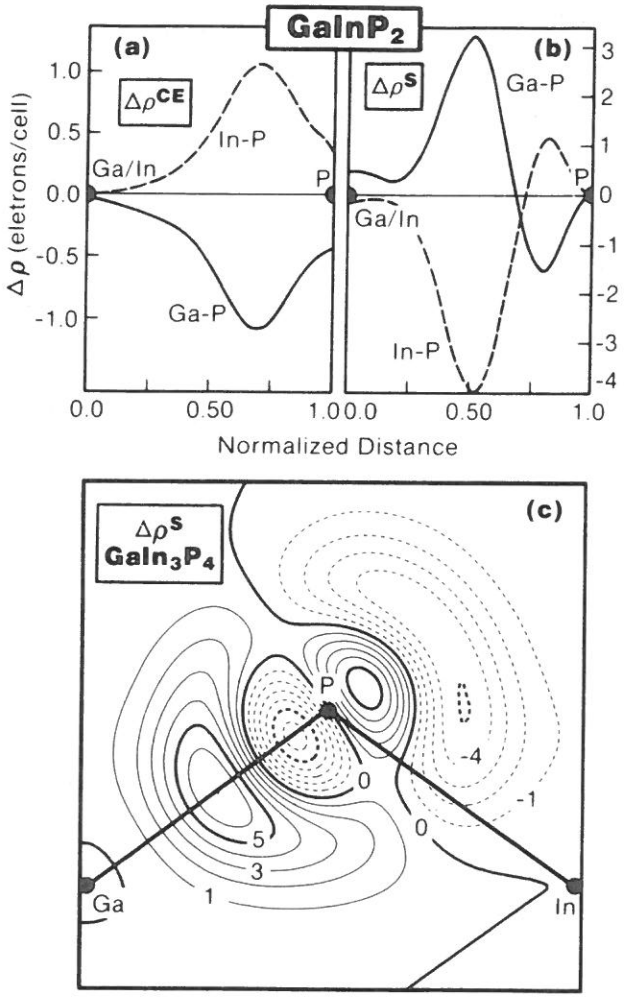


Figure 13. Cation-electronegativity induced [$\Delta\rho^{CE}$ in (a) *c.f.* Eq. (2b)], and structurally induced [$\Delta\rho^{S}$ in (b) *c.f.* Eq. (3b)] changes in the electronic charge densities along the anion-cation bond in $GaInP_2$. (c) shows $\Delta\rho^{S}$ for $GaIn_3P_4$, where solid (dashed) contours indicate gain (loss) of charge.

are: $(\pm 1,0,0)$ and $(\pm 1,\pm 1,0)$ for Luzonite, $(0,\pm 1,\pm 1/2)$ for Chalcopyrite, whereas both the Famatinite and the simple tetragonal structures have in common the $(0,0,\pm 1)$ and $(\pm 1,\pm 1,0)$ beams, but the former also has the $(\pm 1,0,\pm 1/2)$ beam. Third, our analysis suggests that alloys formed from closely lattice matched binaries with a large difference in bond stability in the direction of the charge flow (e.g., $Al_xGa_{1-x}As$ with an $\sim 0.1\%$ bond length mismatch but a large, 24 Kcal/mole excess bond energy of AlAs over GaAs) will order readily below $T_0$ as $(\Delta E^{VD}+\Delta E^{VFF})$ is a vanishingly small positive quantity but $(\Delta E^{CE}+\Delta E^{pol})$ is larger and negative. Ironically, it is this closeness in atomic size (i.e., "atom indistinguishability"), that also renders the same alloy *grown above* $T_c$ as strongly disordered. An opposite example ($\Delta E_0 > 0$) is likely to be $Ga\ Sb_xP_{1-x}$.

We have calculated the changes in the lowest band gaps of $Ga_{4-n}In_nP_4$ relative to the average of the calculated GaP and InP band gaps ("optical bowing") for $n=1,2$ and 3. We find that most of the observed ($b \cong 0.5$ eV) is accounted for by the calculated *VD*, *CE* and *S* changes (0.45 eV). Hence, positive optical bowing can be produced by local bond relaxation effects and need not reflect a thermodynamic instability of the compound. This was shown previously in an earlier study [17].

## X. Enthalpies of Random Alloys

At the temperatures that semiconductor alloys are usually grown, entropy-favored disordered alloys are quenched-in. We model the excess enthalpy of formation $\Delta H_D(x)$ of Eq. (7b) of such substitutionally disordered alloys by assuming the $A_{4-n}B_n$ units to exist at each composition $x(\bar{a})$ with a random probabilities $P^{(n)}[x(\bar{a})] = \binom{4}{n} x^n (1-x)^{4-n}$, [Fig. 14(a)] leading to

$$\Delta H_D(x) = \sum_{n=0}^{4} P^{(n)}[x(a)]\, \Delta E^{(n)}[a,\Delta] \,. \tag{8}$$

The properties of $P^{(n)}(x)$ and $\Delta E^{(n)}(a)$ are such that $\Delta H_D(1) = \Delta H_D(0) = 0$.

Figure 14 shows schematically why $\Delta H_D(x)$ is positive for disordered semiconductor alloy, although stable ordered intermediate phases (i.e., $\Delta E_{eq}^{(n)} < 0$) can exist for integer $A/B$ ratios at lower temperatures. At any given composition, say $x = 1/2$ [at which $\bar{a}(1/2) = a_{AC}^0/2 + a_{BC}^0/2$], the $P^{(2)}(1/2) = 37.5\%$ of the $ABC_2$ species present is seen to be near equilibrium in its $\Delta E^{(2)}(a)$ curve, contributing therefore a negative term to $\Delta H_D$. However, the $P^{(0)}(1/2) = P^{(4)}(1/2) = 6.25\%$ of the pure $AC$ and $BC$ species

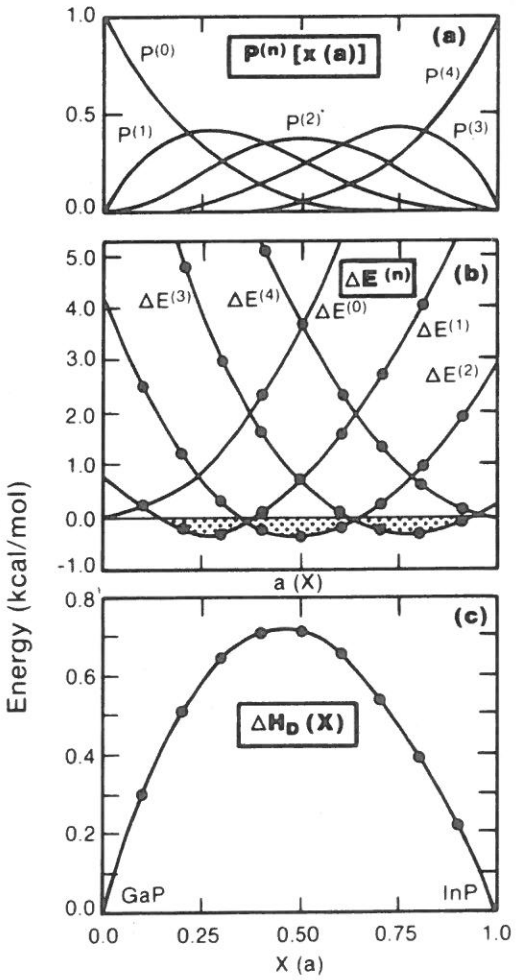


Figure 14. Illustration of the way in which (a) the random occurance probabilities $P^{(n)}(x)$ combine with (b) the equations of state $\Delta E^{(n)}(a)$ of the stable species $n$ (stable areas highlighted by shading), to produce (c) a positive excess enthalpy $\Delta H_D(x)$ of the randomly disordered ($D$) structure.

present at this concentration with $\bar{a}(1/2)$ (as well as the 25% each of the $A_3BC_4$ and $AB_3C_4$ species) are strained relative to their equilibrium lattice constants $a^0_{AC}$ and $a^0_{BC}$, contributing therefore positive terms to $\Delta H_D$. The superposition of all five equations of state $\Delta E^{(n)}$ [Fig. 14(b)], weighted with their probabilities $P^{(n)}[x(\bar{a})]$ [Fig. 14(a)] produce in this case a positive $\Delta H_D(x)$ curve [Fig. 14(c)]. Since we showed that $a^{(n)}_{eq} \cong \bar{a}(n)$, the lattice mismatch $\delta^{(n)}(x)$ of each species in the alloy is $a^{(n)}_{eq} - a(x) = (x - n/4)(a^0_{AC} - a^0_{BC}) \equiv (x - n/4)\Delta a$. For small $\Delta a$, the energy $\Delta E^{(n)}$ is second order in $\delta^{(n)}(x)$, hence $\Delta H_D(x) \sim \Delta a^2$. This is exactly the scaling found empirically [11] to be necessary to explain the distribution of the experimentally measured $\Delta H_D$ values of most semiconductor random alloys.

For $Ga_xIn_{1-x}P$, we find that the experimental [18] $\Delta H_D(x)$ curve for the disordered alloy, with a maximum at $\Delta H_D(1/2) = 0.72$ Kcal/mole (experimental uncertainty in this value is around [11,18] 50%) is consistent with an excess stability of an ordered $GaInP_2$ of $\Delta E^{(2)}_{eq} = -0.3$ kcal/mol.

We can use our calculated bond lengths $R^{(n)}_{AC}(a)$ and $R^{(n)}_{BC}(a)$ for the ordered structure, to obtain their sample-averages $\bar{R}(x)$ in a disordered alloy

$$\bar{R}_{AC}(x) = \sum_{n=0}^{4} \omega^{(n)}_{AC} P^{(n)}[x(a)] R^{(n)}_{AC}(a) , \tag{9}$$

where $\omega^{(n)}_{AC} = 4 - n$ [or $\omega^{(n)}_{BC} = n$] is the number of $AC$ (or $BC$) bonds. A similar expression pertains to $\bar{R}_{BC}(x)$. The dashed lines in Figure 12 show the calculated results, indicating a bimodal distribution similar to that observed for other alloys [5], but $\bar{R}(x)$ a random alloy deviate from the corresponding $d^0$ values significantly more than the bond lengths $R^{(n)}$ in the ordered phases do.

## XI. Summary

Our studies suggest that:

(i) The band gap anomaly in ternary chalcopyrites arises from the response of the band structure to bond alternations $\Delta E^S_g$, and from p-d hybridization effects $\Delta E^{pd}_g$.

(ii) In turn, the bond alternations are decided by the classical atomic size mismatch, and can be calculated in a Paulingesque fashion. Combining (i) and (ii) allows us to predict gaps and structures of numerous new ternary compounds (Table III).

(iii) Optical bowing in pseudobinary alloys made up of size-mismatched species (e.g., $Ga_xIn_{1-x}P$) or electronegativity and size mismatched species (e.g., $ZnS_xTe_{1-x}$) arises from the same structural effect $\Delta E^S_g$ underlying (ii) above, as well as from a chemical electronegativity effect $\Delta E^{CE}_g$. In random alloys made up from nearly equal size atoms (e.g., $Al_xGa_{1-x}As$), the bowing is decided by disorder effects, not local chemical order.

(iv) The chemical energy $\Delta E^{CE} + \Delta E^{\text{pol}}$ decides the magnitude of the cohesive energy, but has little effect on the structural parameters. These can be calculated with useful precision both for isovalent impurities (Fig. 8) and for ternary chalcopyrites (Figs. 6 and 7) from strain-minimizing models.

(v) The stability of the ordered structures arises from the fact that they are *strain-reducing* (i.e., small $\Delta E^{VD} + \Delta E^{\text{VFF}}$), reflecting their ability to simultaneously accommodate the two dissimilar bond lengths in a coherent fashion (solid circles in

Fig. 12). When small, this allows the stabilizing chemical charge transfer terms to take over (the net electron flow is from the less stable bond to the more stable bond). Such ordered systems are predicted to have a Vegard-like lattice constant, much like their random analogs at the same concentration (hence the latter could be used as a convenient substrate for growing the former), a sharp bimodal distribution of bond lengths with displaced anions, and positive "optical bowing" (although with somewhat larger gaps than their random counterparts).

(vi) In contrast, random alloys do not minimize strain: although the *average* bond lengths are still close to the ideal bonds (solid squares in Fig. 12), configurations with strained bonds are quenched-in [Fig. 14(b)]. They are entropy stabilized over the ordered phase when grown at temperatures above $T_c$ or ($T_0$), hence annealing of these samples is not likely to order them readily. Upon quenching to lower temperatures they will either (a) disproportionate, (b) remain metastably disordered, or (c) order. Ordering and disproportionation can occur if sufficient atomic mobility remains at the lower temperature and the activation barriers posed, for example, by coherent strains [11], are surmountable. The choice between these two reactions depends both on the relative values of $T_c$ and $T_0$ and on the relative size of their (unknown) activation barriers. While reaction (c) could hopefully be catalyzed chemically or by suitable photons, under normal condition, reaction (a) (e.g., in Ga $P_xSb_{1-x}$, showing a miscibility gap) or (b) (e.g,. in $Ga_xAl_{1-x}As$) prevail upon cooling. However, if grown *from the outset* below $T_0$ (about $\Delta E_0/k \cong 200°C$ below conventional growth temperatures) by growth technique that assures sufficient surface mobilities at lower temperatures, ordered phases, presumably with appealing transport properties, are predicted to form.

After the completion of this work, two experimental groups have succeeded in growing, for the first time, *ordered semiconductor alloys*. The first [19] grew $Al_xGa_{1-x}As$ and the second [20] obtained $InGaAs_2$. The Growth of $Al_xGa_{1-x}As$ was done as a *continuous* (homogeneous) process, i.e., without forcing artifical symmetry through the growth process. Nevertheless, an ordered structure was obtained [19]. Although this ordering may have been established kinetically, the authors presented evidence that in fact the ordered phase is the thermodynamic equilibrium state at low temperatures, as predicted before [14]. These structures show the expected [14] diffraction spots and long range order. They hold the promise of becoming new, stable and high-mobility semiconductors with convenient energy band gaps.

## Bibliography

[1] *GaInAsP Alloy Semiconductors*, T. P. Pearsall, Ed. (Wiley, New York, 1982).
[2] J. E. Jaffe and A. Zunger, Phys. Rev. B **29**, 1882 (1984); *ibid* **27**, 5176 (1983).
[3] S. Larach, R. E. Schrader and C. F. Stocker, Phys. Rev. **108**, 587, (1957).
[4] A. G. Khachaturyan, *Theory of Structural Transformations in Solids*, (Wiley, New York, 1983).
[5] J. C. Mikkelsen and J. B. Boyce, Phys. Rev. Lett. **49**, 1412 (1983).
[6] P. Bendt and A. Zunger, Phys. Rev. B **26**, 3114 (1984); J. E. Jaffe and A. Zunger, Phys. Rev. B. **28**, 5822 (1983).

[7] J. E. Jaffe and A. Zunger, Phys. Rev. B **30**, 471 (1984).
[8] J. L. Martins and A. Zunger, Phys. Rev. B **30**, 6217 (1984).
[9] *e.g.*, J. A. Van Vechten and T. K. Bergstresser, Phys. Rev. B **1**, 3351 (1970); D. Richardson, J. Phys. C **4** L289 (1971); A. B. Chen and A. Sher, Phys. Rev. Lett. **40**, 900 (1978); W. Porod and D. K. Ferry, Phys. Rev. B **27**, 2587 (1983).
[10] P. A. Fedders and M. W. Muller, J. Phys. Chem. Solids **45**, 685 (1984).
[11] G. B. Stringfellow, J. Crys. Growth **27**, 21 (1974); J. Elect. Mat. **11**, 903 (1982).
[12] J. Van Vechten in *Semiconductors Handbook,* S. P. Keller, Ed. (North Holland, Amsterdam, 1980), Vol. **3**, pp. 1.
[13] J. Ihm, A. Zunger and M. L. Cohen, J. Phys. C **12**, 4409 (1979).
[14] G. P. Srivastava, J. L. Martins and A. Zunger, Phys. Rev. B (In Press, Feb. 15, 1985).
[15] S. Froyen and M. L. Cohen, Phys. Rev. B **28**, 3258 (1983).
[16] H. G. Brühl and U. Pietsch, Phys. Stat. Solidi **68A**, 689 (1981).
[17] A. Zunger and J. E. Jaffe, Phys. Rev. Lett. **51**, 662 (1983).
[18] I. V. Bodnar, E. E. Matjas and L. A. Makovetskaya, Phys. Stat. Solidi **36A**, 12141 (1976).
[19] T. S. Kuan, T. F. Kuech, W. I. Wang and E. L. Wilkie, Phys. Rev. Lett. (In Press).
[20] T. Fukui and H. Saito, Jap. J. Appl. Phys. L **521** (1984).

Received May 20, 1985